Large-area lasing and multicolor perovskite quantum dot patterns

Chun Hao Lin[1], Qingji Zeng[2], Evan Lafalce[2], Shengtao Yu[1], Marcus J. Smith[1,3], Young Jun Yoon[1], Yajing Chang[1,4], Yang Jiang[4] Zhiqun Lin[1], Z. Valy Vardeny[2], & Vladimir V. Tsukruk[1*]

[1]School of Materials Science and Engineering, Georgia Institute of Technology, Atlanta, Georgia 30332, USA

[2]Department of Physics and Astronomy, University of Utah, Salt Lake City, Utah 84112, USA

[3]Aerospace Systems Directorate, Air Force Research Laboratory, Wright-Patterson Air Force Base, Ohio 45433, USA

[4]School of Materials Science and Engineering, Hefei University of Technology, Hefei, Anhui 230009, P. R. China

Abstract

We report a novel orthogonal lithography fabrication of patterned inorganic perovskite $CsPbX_3$ (X= Cl, Br, I) quantum dot (QD) arrays which cannot be patterned with traditional approaches. This approach involves a combination of fluorinated polymer and solvent to resolve issues of polar-non-polar solvent constraints thus enabling the fabrication of complex patterns with high optical gain and bright and multicolor emission. We utilized this approach to fabricate high-resolution large-area arrays of microdisk lasers and milticolor (binary- and ternary- emission) pixels. The optical cavity modes of $CsPbBr_3$ QD microdisk lasers were readily controlled by tuning the disk size, where the mode spacing decreases while the number of modes increases with increasing disk diameter. Finally, we demonstrated the versatility of our approach for the integration of environmentally-sensitive QDs with different emission signatures and composition on the same chip, while achieving high density, high-resolution large-area QD arrays with multicolor pixels.

*** Corresponding author:** Vladimir@mse.gatech.edu

Keywords: perovskite quantum dots, microdisk lasers, whispering gallery modes, orthogonal lithography, multicolor pixel arrays

1. Introduction

Recently, a new class of semiconductor nanocrystals, namely, all-inorganic perovskite $CsPbX_3$ (X=Br, Cl, I) quantum dots (QDs), has attracted great attention due to their intriguing optical, chemical, and lasing properties. [1,2,3,4] Unlike more conventional Cd based QDs, $CsPbX_3$ QDs do not require shell passivation to achieve high quantum yield due to the self-passivation effect of halogen, [5,6] enabling a facile synthesis of highly fluorescent emitters without the need of careful design of core/shell interface. [7,8] In addition, the absorption and emission spectra of QDs can be altered not only by size but also by the facile composition tuning via anion (i.e., X) exchange, thereby providing more freedom to achieve superior optical properties. [9] Moreover, high net optical gain value of 450 cm^{-1} and low pump threshold down to 5 $\mu J/cm^2$ have been reported, demonstrating that these QD can be readily used for light amplification and lasing at very low excitation intensity. [10] These properties have been extensively studied for use in spectrochemical probes, light-emitting diodes, and vertical cavity surface emitting lasers. Clearly, these show that $CsPbX_3$ QDs have potential for a variety of optoelectronic applications. [11,12,13]

In recent years, patterning techniques for single crystal and polycrystalline perovskite materials have been extensively developed including electron beam lithography, controlled crystallization via molding, inkjet printing and template assisted patterning with intriguing photonic properties. [14,15,16,17,18,19] In contrast, nearly all studies of perovskite nanoparticles such as QDs to date have focused on the synthesis, photophysics and optoelectronic applications while the development of patterning techniques has been comparatively few and limited in scope. [20,21] This approach contrasts sharply to the Cd-based QDs where high-resolution lithographic methods such as electron-beam lithography and photolithography have been adopted widely to integrate Cd-based QDs into micro- and nanoscale devices. [22,23] The difference is essentially understandable, when considering the ionic nature of $CsPbX_3$ QDs, which makes them prone to dissolution in common polar solvents that are required in

these high-resolution lithographic methods.[24,25] The chemical instability to polar solvents severely hinders the integration of these QDs into patterned photonic structures. Moreover, unlike counterpart of the bulk perovskite materials that can be patterned by dissolving polymer spheres or templates with non-polar solvent such as toluene,[19] the ligand-capped perovskite QDs are unfortunately well dispersed in non-polar solvents. The solvent constraint in both polar and non-polar solvents indeed places the development of $CsPbX_3$ QD patterning for miniaturized optical arrays in a dilemma. Clearly, a novel lithographic method should be proposed to effectively overcome the low material processability of $CsPbX_3$ QDs that originates from the solvent constraint, while preserving the ability to achieve large-area high-resolution patterns.

Herein, we report a novel photolithographical approach that overcomes the processing limitations of perovskite QDs by incorporating a fluorinated polymer resist, which provides orthogonality to these QDs during the lift-off process with the fluorinated solvent processing without affecting QD emission performance. The orthogonality and spatial precision of photolithography enable the facile fabrication of large-area arrays of sophisticated patterns with submicron-sized features. We further demonstrated how this patterning technique can be used in different fabrications including QD microdisk arrays with lasing properties and multicolor pixels on the same chip. Furthermore, arrays of microdisk laser arrays with high quality factor of optical cavity modes of 500-700 were successfully fabricated. Finally, we demonstrate the versatility of our approach to integrate QDs with different emission properties into large-area arrays of multicolor microscale patterns with high areal density of ~1000 pixels per inch (ppi). Importantly, this novel patterning approach can be potentially applied to other types of QDs with poor environmental stability for the development of QD-based photonic structures.

2. Results and discussion

2.1. Fabrication of $CsPbBr_3$ QD micropatterns

To fabricate patterns of all-inorganic perovskite quantum dots, we utilized green-emitting $CsPbBr_3$ QDs (see **Experimental** for synthesis procedure). [12] **Figure 1a** shows the basic optical absorption and emission spectra of synthesized $CsPbBr_3$ QD. Transmission electron microscopy (TEM) was used to examine the overall shape and size of the synthesized $CsPbBr_3$ QDs (**Figure S1**). The shape of $CsPbBr_3$ QDs is close to cuboids with the average length and width to be 13.1 ± 1.1 nm and 6.5 ± 0.7 nm, respectively. Generally, we do not observe significant difference in their absorption and emission spectra compared to those of QDs with cubic shape because their dimensions are close/above their Bohr diameter (7 nm) [26], indicating that our QDs are in the weak confinement regime with stabilized optical properties.

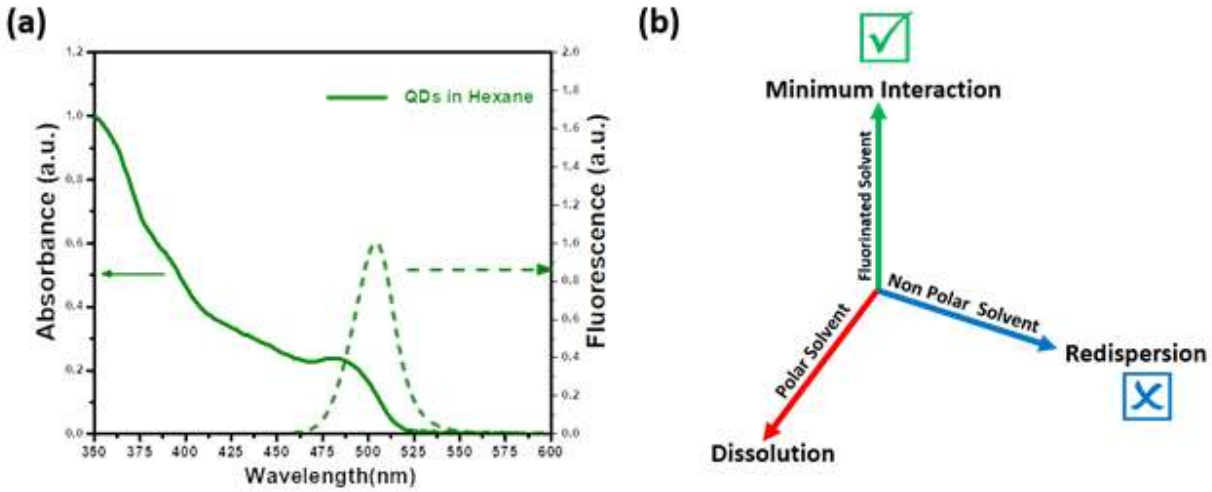

Figure 1. (a) Absorbance and fluorescent emission of $CsPbBr_3$ QDs in hexane. (b) Schematic of solvent constraint of $CsPbBr_3$ QDs.

As known, attempts to purify common perovskite QDs showed that excessive washing steps lead to removal of ligands and insolubility to non-polar solvent, while insufficient washing leads to excessive ligands that are still presented in the final QD solution thus compromising multi-stage lithographical process. [24] Hence, we have

adopted a synthesis method that utilizes only oleic acid as the surface capping agent. [12] This method prevents ligand dynamic binding leading to the facile ligand loss during purification procedures. [12,27] Indeed, as-prepared colloidal solutions show better colloidal stability compared to those synthesized by conventional methods.

Furthermore, to overcome the solvent constraints, the direct exposure of perovskite QDs to polar and non-polar solvents should be avoided during the lithography process since it causes their dissolution (**Figure 1b**). Therefore, we utilize the fluorinated polymer (OSCoR SL 1) as a novel sacrificial layer. [28] This sacrificial layer enables patterning using standard photolithography while providing the orthogonality to $CsPbBr_3$ QDs during lift-off process. Specifically, the fluorinated polymer along with photoresist can be removed by immersing the QDs into the fluorinated stripper which dissolves the underlying fluorinated polymer layer while the $CsPbBr_3$ QD patterns remain intact, because the interaction of the stripper with $CsPbBr_3$ QDs is minimal.

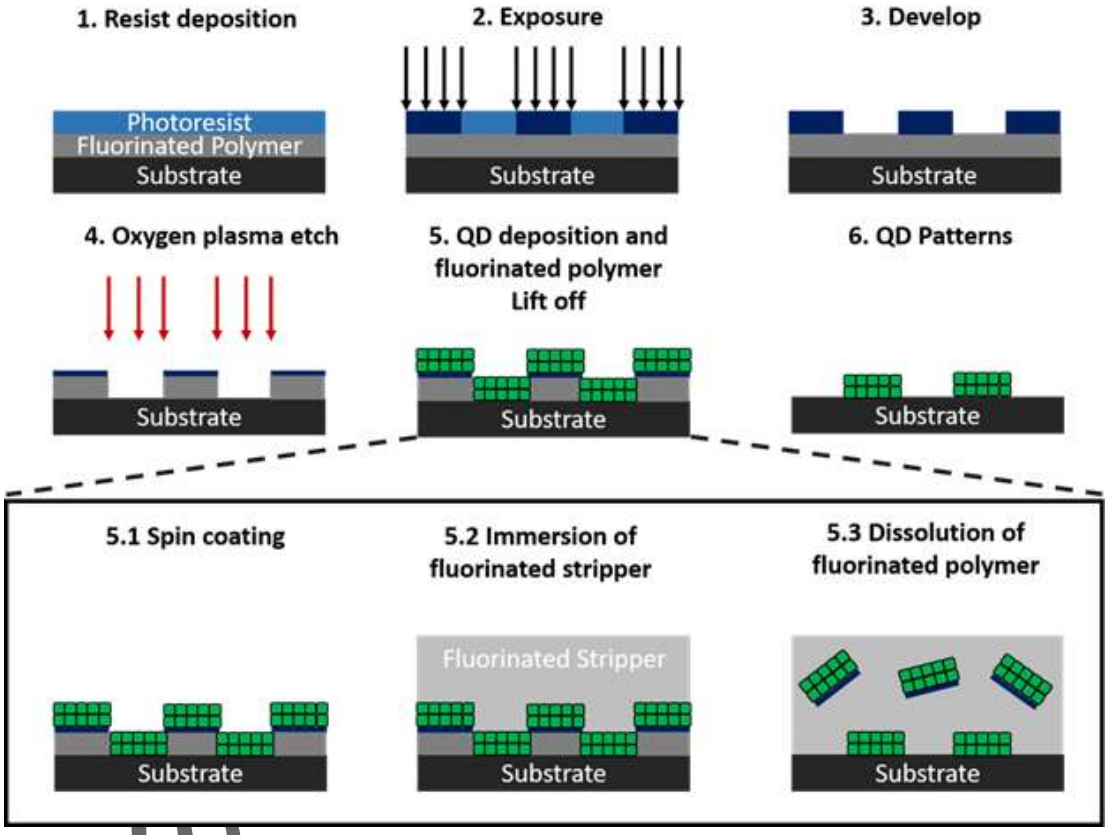

Figure 2. Schematic that outlines orthogonal lithography approach for fabricating $CsPbBr_3$ QD patterns via the insertion of fluorinated polymer layer and standard photolithography.

The orthogonal lithography process includes several steps (**Figure 2**). [29] First, the fluorinated polymer is spin-cast on a substrate as a sacrificial layer (**Figure 2, step 1**). Subsequently, standard photolithography was used to fabricate microscale trenches of predesigned patterns (**Figure 2, step 1-4**). During the patterning process, the photoresist template acted as a mask while an oxygen plasma etch was performed to etch the underlying fluorinated polymer (**Figure 2, step 4**). These patterned trenches were subsequently filled with $CsPbBr_3$ QDs via spin-coating (**Figure 2, step 5.1**). Finally, the fluorinated polymer was dissolved by immersing into the fluorinated stripper while CsPbBr3 QDs attached to the photoresist layer were lifted off (**Figure 2, step 5.2-5.3**) and remained strongly emissive (**Figure 2, step 6**).

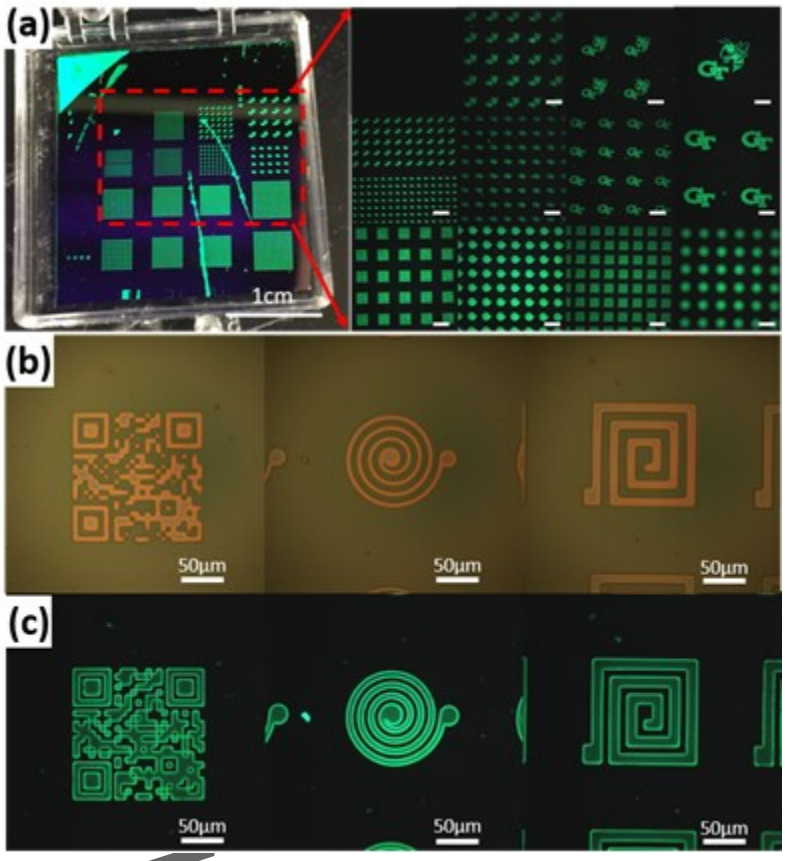

Figure 3. (a) Left panel: Optical micrograph of a substrate under UV illumination with arrays of different QD patterns. Right panel: fluorescent images of QD arrays of different patterns at the corresponding positions. All scale bars are 200 μm. Bright field (b) and fluorescent (c) images of different individual elements.

With this method, large-area (2 cm x 2 cm) arrays of different patterns can be fabricated (**Figure 3a**). Examples of QR codes, circles and square spirals with high emission in green range are shown in **Figure 3b, c and S2**.

2.2. Optical gains of $CsPbBr_3$ QD film

Prior to the investigation of optical mode activity in perovskite microdisks, we conducted measurements to evaluate the lasing properties of assembled uniform $CsPbBr_3$ QD film

using a standard configuration of the variable stripe length (VSL) method with a pulse laser excitation (see Experimental Section). [30]

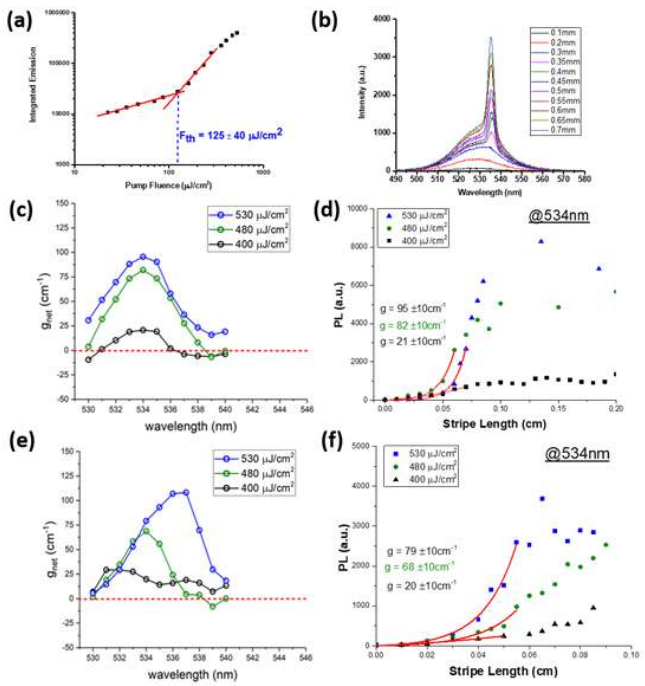

Figure 4. (a) Emission intensity vs excitation fluence response of CsPbBr3 QD film with ASE threshold as noted. (b) Emission spectra of QD film at various stripe lengths. (c) The optical gain spectra and (d) fitted optical gain values at 534 nm for as-prepared $CsPbBr_3$ QD film at various pump fluences. (e) The optical gain spectra and (f) optical gain values at 534 nm of $CsPbBr_3$ QD film after immersion into fluorinated stripper for an hour at various fluences.

Significant spectral narrowing and an exponential increase of the emission intensity indicate mirrorless laser action (**Figures 4a,b, S3a)**. A characteristic the amplified spontaneous emission (ASE) threshold occurs at 125 ± 40 μJ/cm^2 which is lower than previously reported values and close to those extrapolated for femtosecond lasing.[10,31]

Next, net gain values were measured to be as high as 180 ± 25 cm^{-1} in the $CsPbBr_3$ QD films which is higher than that measured for other QD films (**Figures 4c, d, S3b**). [30, 32] Furthermore, we have investigated solvent resistance of the $CsPbBr_3$ QD film, since

$CsPbBr_3$ QD are known to be extremely sensitive to solvents. In fact, the net gain values remained high after immersion into fluorinated stripper for an hour thus enabling the fabrication of $CsPbBr_3$ QDs patterns (**Figure 4e, f**). This is in contrast to fast deterioration of fluorescence after immersion of common photoresists in water for a minute. [33]

2.3 Optical properties and lasing behavior of perovskite microdisks

To study the optical mode activity of $CsPbBr_3$ QD structures, we have fabricated microdisks with various diameters, *D,* from 11.7 to 52.2 μm (**Figure 5**). The QD microdisks were found to possess a nest-like topography, where elevated rims are formed toward the circumference, common for these structures (**Figure 5b**). [34,35]

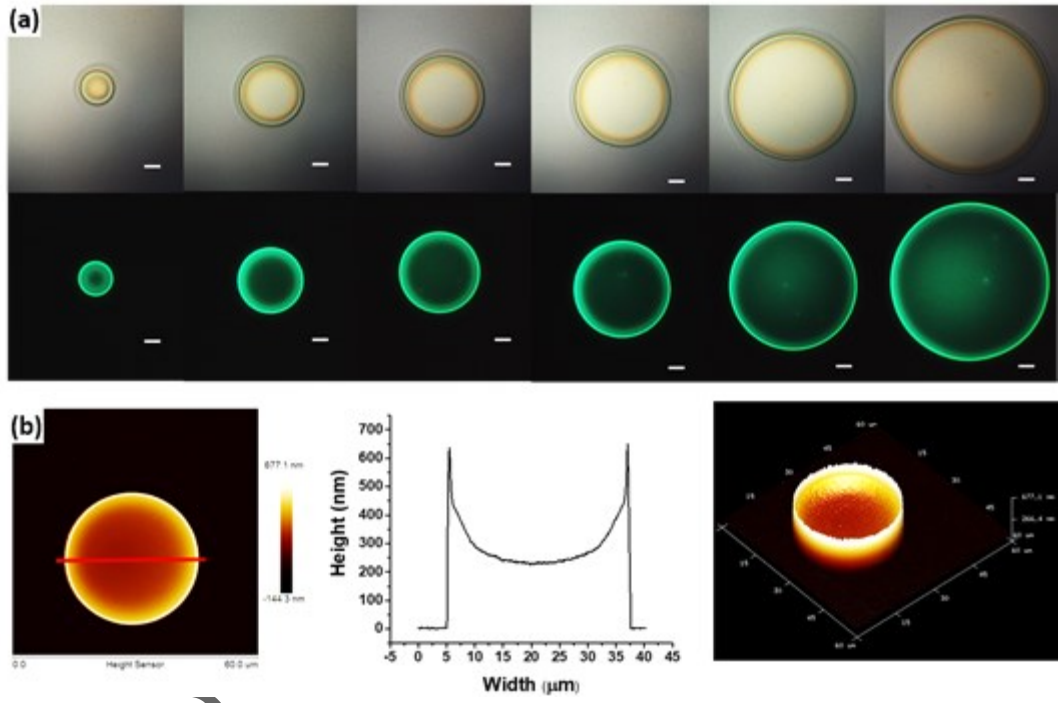

Figure 5. (a) Bright field (top) and fluorescent (bottom) images of QD microdisks with diameters of 11.7, 21.8, 26.7, 31.8, 41.6 and 52.2 μm. All scale bars are 5 μm (b) From left to right: AFM topographical image (top-view), height profiles, and 3D image of QD microdisk with diameter of 31.8 μm.

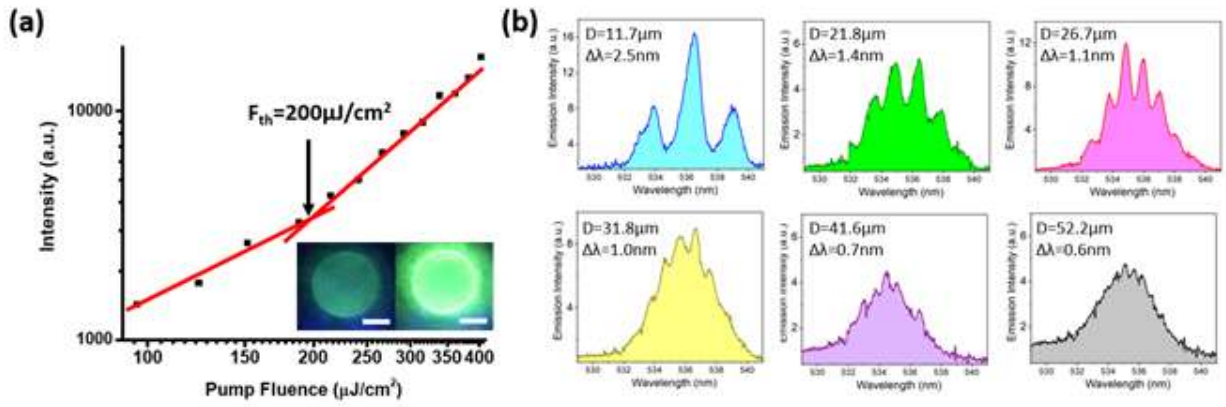

Figure 6. (a) Emission intensity vs. excitation fluence measured from a $CsPbBr_3$ QD microdisk. The threshold intensity, F_{th} is determined from the interception of the linear and superlinear responses. Inset: PL images of QDs microdisk (D = 26.7 μm) below (left) and above (right) lasing threshold. The scale bar is 10 μm for both images. (b) Lasing spectra of QD microdisks with D = 11.7 μm, 21.8 μm, 26.7 μm, 31.8 μm, 41.6 μm and 52.2 μm, respectively. Δλ is the average 'mode spacing' of the observed longitudinal cavity modes.

The QD microdisks fabricated here display intense localized emission, suggesting strong waveguiding and efficient cavity optical mode generation (**Figure 6**). A non-linear behaviour was observed with increasing pump fluence, where the threshold intensity was determined to be ~200 μJ/cm^2 (**Figure 6a**), a value similar to threshold values observed for the pristine QD film. In addition, sharp spectral peaks appeared over the broad spontaneous emission band once the pump fluence exceeds the threshold value (**Figure 6b**). All of these findings confirm the preservation of optical lasing activity and total internal reflection near the disk circumference. The cavity mode spacing (Δλ) was found to decrease with increasing disk diameter, while the number of resonant longitudinal cavity modes increases in agreement with theoretical predictions (**Figure 6b**). [36,37,38]

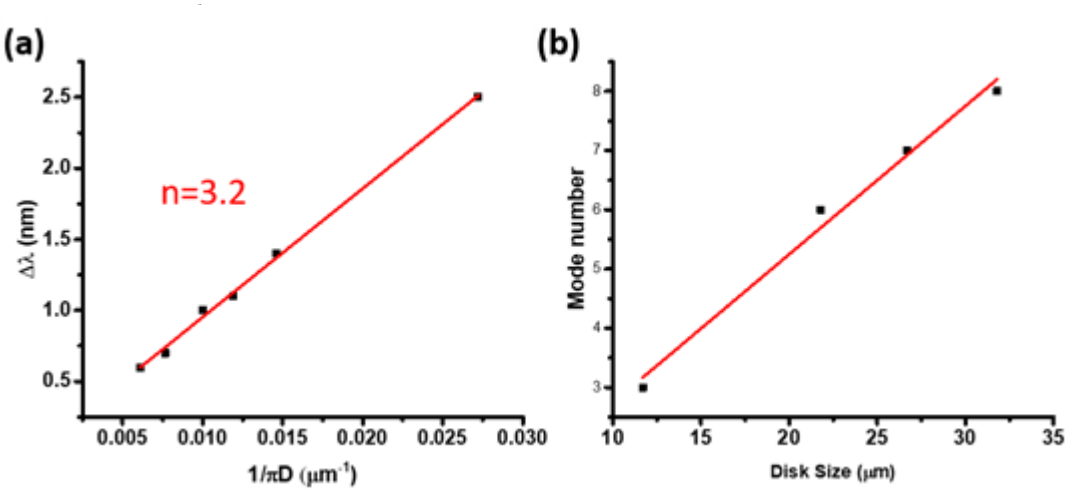

Figure 7. (a) The mode spacing, $\Delta\lambda$ of the WG modes in QD micridisk lasers with various diameter, D vs. the reciprocal geometrical path length, $1/\pi D$. The group index, n is calculated from the relation: $\Delta\lambda = \lambda^2/n\pi D$. (b) The plot of mode number versus the disk size.

This trend is also confirmed by the linear relationship between the cavity mode spacing ($\Delta\lambda$) and the reciprocal optical path length $1/n\pi D$, according to the relation, $\Delta\lambda = \lambda^2/n\pi D$ which is expected for circular microcavity (**Figure 7a**). [36] From this relationship, the group index, n of the $CsPbBr_3$ QDs microdisks was estimated to be 3.2 which is larger than the bulk refractive index of $CsPbBr_3$ (n=2.3). [45] The enhancement in refractive index may be attributed to the exciton-photon coupling that has been discovered in single crystalline perovskites, which should be further investigated in the future. [39,40]

Moreover, the mode number can also be estimated by using lasing spectra of microdisks with different sizes and their corresponding mode spacing. The mode number was estimated to be 3, 6, 7 and 8 for disk size of 11.7 μm, 21.8 μm, 26.7 μm and 31.8 μm. It is noteworthy that the mode number for disk size of 41.6 μm and 52.2 μm can not be exactly estimated since line widths of cavity modes (~0.8-1 nm)

are already larger than the mode spacing (0.6-0.7 nm). As expected, the number of modes increases proportionally with the increasing disk size. Therefore, multimode operation with specific set of modes is possible by carefully defining the disk size. [41] In addition we suggest that a single-mode lasing may be possible by reducing the disk size to a diameter that is small enough to support only one cavity mode or engineering the shape of lasing structures with suppressed secondary modes. Parity-time symmetry is another interesting possibility where coupled lasing structures with balanced gain and loss can achieve the exceptional point with only one specific cavity mode amplified. [42]

Furthermore, the quality factor, Q, for microdisks fabricated here can be estimated from the relation $Q = \lambda/\delta\lambda$, where λ is the peak wavelength of the cavity mode and $\delta\lambda$ is its line width. [36] The high quality factor of the dominant modes in QD microdisks with different diameters within the range of 500-700 is comparable to that reported from microcavities of perovskite single crystals. [43,44] However, these single crystal perovskites are grown with random size, geometry and location that excludes fabrication of large-area organized photonic arrays. [45] In contrast, the precise control the spatial organization of QD microstructures at large scale is facilitated by the photo-lithographical approach.

2.4. Dual color pixel arrays

In addition to single emission signature microdisk lasers we applied two-stage orthogonal lithography process to fabricate dual color arrays by combining QDs with different emission signature (**Figure 8**). The process flow includes the fabrication of first pattern of circular structures (D=~11.7 μm) made of green $CsPbBr_3$ QDs (**Figure 2**). Next, the second complementary pattern was fabricated from red-emitting $CdSe/Cd_{1-x}Zn_xSe_{1-y}S_y$ QDs by using the same orthogonal lithography process and the mask aligner for positioning microdisks. The standard photolithography was again used to create a secondary photoresist mask on top of the fluorinated polymer with embedded prior fabricated structures (**Figure 8, step 1-3**).

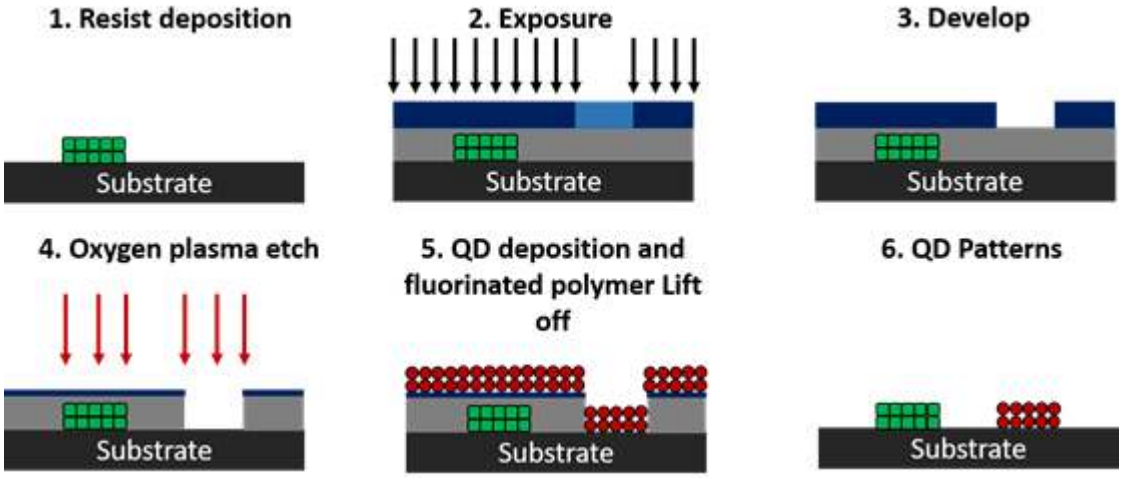

Figure 8. Schematic that outlines the orthogonal lithography approach that is used multiple times for fabricating dual-color patterns of QDs.

During the second lithography process, the $CsPbBr_3$ QD patterns were fully protected by the fluorinated polymer and hence maintained their structure integrity. Fluorinated polymer not covered by photoresist was etched by plasma etching, generating local trenches on the substrate (**Figure 8, step 4)**. Red-emitting $CdSe/Cd_{1-x}Zn_xSe_{1-y}S_y$ QDs were further deposited via spin-coating and the fluorinated polymer was then dissolved by immersing into the fluorinated stripper (**Figure 8, step 5)**. Lastly, the photoresist was lifted off leaving patterns of red $CdSe/Cd_{1-x}Zn_xSe_{1-y}S_y$ QDs on the substrate that are close to the first set of green $CsPbBr_3$ QD structures (**Figure 8, step 5-6)**.

The initial fabricated array shows intense green emission from $CsPbBr_3$ QD circular structures (**Figure 9a**). After the second stage, the orange color appeared due to the mixed green and red QD emissions, indicating a successful integration of two different QD arrays onto the same chip (**Figure 9b**). Indeed, the higher resolution fluorescent image shows microscale pixels that consist of binary pixels of closely packed green and red QD circles (**Figure 9c**). Each pixel size is 25 μm x 25μm that corresponds to a density of ~1000 ppi, a value that is higher than the resolution of

the current phone displays which is typically 200-500 ppi (e.g., 264 ppi for Retina Display in iPad display). [46]

Furthermore, optical properties of these circular structures including emission spectrum and spatial distribution of PL intensity within a single pixel were studied using high-resolution hyperspectral system. PL emissions of green and red patterns were centered at 510 nm and 623 nm with full-width half maximum of 22 nm and 40 nm, respectively (**Figure S4**). Moreover, the spatial distribution of PL intensity for both green and red patterns were found to be nest-like with the PL intensity in the middle region is approximately 30-40% of the maximum PL intensity at the rim (**Figure 9d**). These spatial distributions of PL intensity have similar characteristics to the microdisk topography indicating the physical dimension of microscale patterns controls the spatial distribution of PL intensity (**Figure 3b**).

Importantly, blue CdSe/$Cd_{1-x}Zn_xSe_{1-y}S_y$ QDs with PL emission centered at 467nm (**Figure S5**) can also be integrated to form the third set of circle patterns by using our approach repeatedly. **Figure 9e** demonstrated the preliminary result of RGB arrays with three sets of QD patterns that emit at blue, green and red region, respectively. Further optimization of our fabrication process can be done in the future to improve the alignment between patterns. This capability can strongly support the realization of high-resolution QD optoelectronic devices with miniaturized pixels including full-color QD light-emitting diodes and photodetectors that require pixels consisting of QD components with precisely controlled emission and absorption properties. [12,47,48]

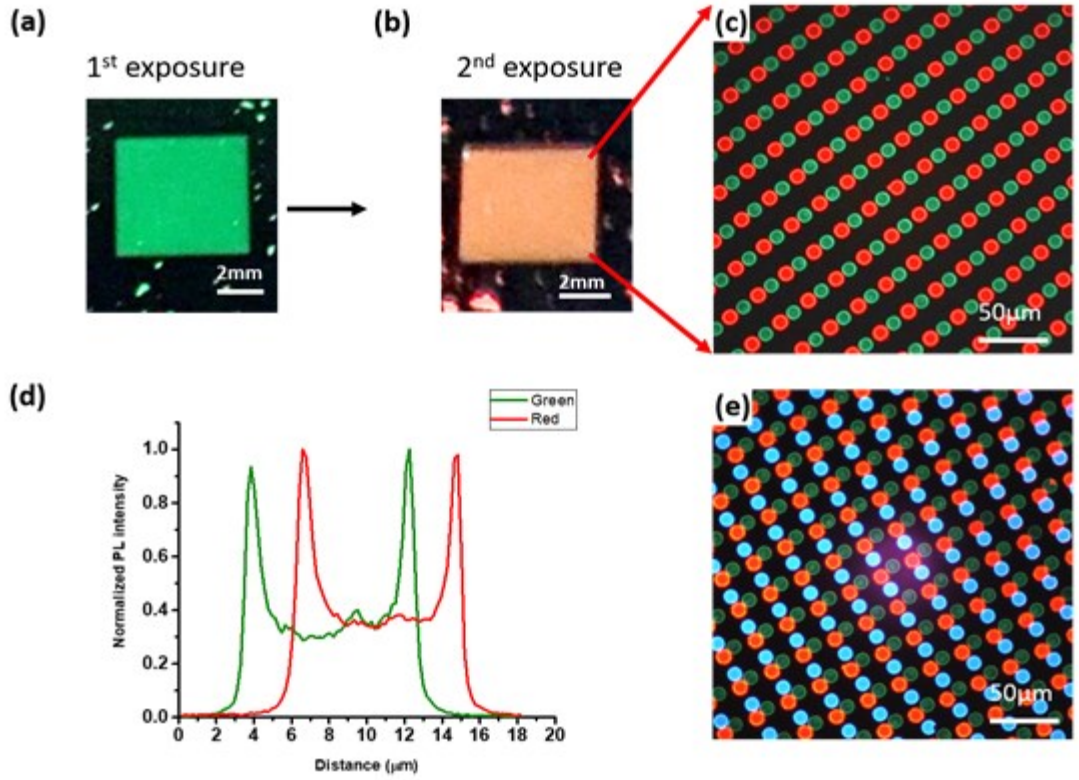

Figure 9. (a) Fluorescent image of an array of $CsPbBr_3$ microdisks. (b) Fluorescent image of the binary array of $CsPbBr_3$ QDs (green) and $CdSe/Cd_{1-x}Zn_xSe_{1-y}S_y$ QDs (red) microdisks and corresponding high-resolution fluorescent image (c). (d) Spatial distribution of PL intensity for ~11.7 μm individual green and red QD microdisks. (e) Fluorescent image shows the preliminary result of RGB arrays of red, green and blue QD patterns using our approach.

3. Conclusion

In summary, we fabricated high-resolution, large-area patterning of environmentally-sensitive perovskite QDs for efficient lasing structures and multicolor (binary and ternary color) emitting pixel arrays. The utilization of fluorinated photoresist and solvents allows to avoid easy dissolution and damaging of perovskite QDs during the multi-stage lithographical process. This approach preserves the high optical gain performance of QDs film and efficient optical lasing of circular QD microstructures with high quality cavity modes. Furthermore, we have demonstrated the multicolor emission arrays with paired circular microstructures of green, blue, and red-emitting QDs and high areal density of ~1000 ppi, much higher than common display resolution. These parameters are higher than that known for many pixelated arrays such as high-resolution displays and full-color QD light-emitting diodes with pixels

containing QD components with different emissions for potentially full color displays. [12,48] Importantly, this approach can be potentially applied to other types of semiconducting nanocrystals with poor environmental stability for the development of QD-based photonic structures.

4. Experimental

Chemicals and materials: Cadmium oxide, tri-n-octylphosphine (TOP, 90%), and selenium powder, were obtained from Sigma Aldrich. Cesium acetate (99.9%), Lead acetate trihydrate (99.995%) and tetra-n-octylammonium bromide (TOABr) (98+%) were obtained from Alfa Aesar. 1-octadecene (ODE, 90%), oleic acid (OA, 97%), and bis(trimethylsilyl) sulfide (95%) were obtained from TCI and ethyl lactate was obtained from Sigma Aldrich. Hexane, acetone, toluene (ACS reagent grade) and heptane were obtained from BDH Chemicals. CYTOP was obtained from AGC Chemicals. NR 71-3000p photoresist was purchased from Futurrex. OSCoR SL 1 (fluorinated polymer), thinning solvent 700 and Orthogonal Stripper 700 (fluorinated stripper) were purchased from Orthogonal, Inc. All chemicals were used as received.

Synthesis of $CsPbBr_3$ QDs: $CsPbBr_3$ QDs were synthesized by modifying the reported method. [12] 1 mmol of cesium acetate, 2 mmol of lead acetate trihydrate, 5 ml of ODE, and 2 ml of OA is added into a three neck flask. The solution is vacuum dried at 100°C for 30 minutes and then changed to argon atmosphere at 75°C. 2 mmol of TOABr is dissolved in anhydrous toluene and oleic acid. The TOABr solution is injected into the three-neck flask. After 10 seconds, the heating mantle is removed and cooled in a water bath. The as-prepared $CsPbBr_3$ QD solution was purified by adding acetone at a ratio of 1:2 (toluene:acetone) and subsequently centrifuged at 10000 rpm for 30 min. This washing step was performed twice. The supernatant was discarded and the purified $CsPbBr_3$ QDs were redispersed in heptane (2 ml). The QD solution was centrifuged at 8000 rpm for 10 min to remove any possible aggregates in solution and the remaining supernatant was used as the final $CsPbBr_3$ QD solution.

Synthesis of compositional gradient $CdSe/Cd_{1-x}Zn_xSe_{1-y}S_y$ QDs: gradient $CdSe/Cd_{1-x}Zn_xSe_{1-y}S_y$ core/graded-shell QDs were synthesized by modifying reported methods.[49] Briefly, 0.2 mmol of CdO, 4 mmol of $Zn(acetate)_2$, 5 ml of oleic acid, and 15 ml of 1-octadecene (ODE) were placed in a three-neck flask and degassed at 150°C for 1 hr. The reaction was heated to 300°C under Ar. At the elevated temperature (300°C), 1 mmol of Se and 4 mmol

of S in 2 ml of TOP were rapidly injected into the reaction vessel. The reaction was allowed to proceed at 300°C for 10 minutes, and then the heating mantle was removed to stop reaction. 5 ml of hexane was added to the solution once the temperature reached 70°C.

Optical characterization: UV-vis extinction spectra of QD solutions in quartz cuvette from 350-900 nm were collected using a Shimadzu UV-vis-2450 spectrometer with D2 and tungsten lamps offering a wavelength range of 300-1100 nm. The QD extinction spectra were corrected against the pure solvent background and the same quartz cuvette. Photoluminescence spectra of QD solutions were collected using a Shimadzu RF-5301PC spectrofluorophotometer with the excitation wavelength of 480 nm to excite $CsPbBr_3$ QDs that are dissolved in hexane.

Photoluminescence (PL) images were collected using CytoViva hyperspectral system with a Dagexcel-M Digital Firewire camera (cooled) installed on optical microscope (Olympus bx51) and a 50x objective, as outlined in previous works. [50,51] PL imaging was performed using photoluminescence excitation from a blue bandpass filter (450-490 nm) with a dichroic mirror that reflects optical wavelengths below 495 nm, and with a longpass emission filter that passes optical wavelengths above 500 nm. The light source is a quartz halogen lamp with an aluminum reflector providing a wavelength range of 420−850 nm and a power of 150 W of unpolarized light.

Gain measurements: The third harmonic (355 nm) of a Spectra Physics Quanta-Ray INDI-series Pulsed Nd:YAG laser (pulse width of 7 ns, repetition rate of 10 Hz) was used directly as a seed for a GWU-Lasertechnik basiScan Beta-Barium Borate Optical Parametric Oscillator (OPO), producing tunable pulses of 450nm with 10μJ maximum pulse power (pulse width of 7 ns). For the variable stripe length (VSL) gain measurements, the excitation beam was shaped into a stripe of 125 μm width using a cylindrical lens (15 cm focus length), and the stripe length was controlled by a pair of blades mounted on mechanically controlled stages that provided an adjustable slit. Only the central 10 % of the beam was used to minimize pump inhomogeneity due the Gaussian intensity profile. The pump beam intensity, I_p, was varied by means of a pair of polarizers. One end of the stripe excitation was placed on the cleaved edge of the film while the length of the excitation stripe was progressively increased. The emission from the edge was collected with a 1 mm diameter fiber and recorded using a commercial spectrometer (Ocean Optics USB4000; resolution 2 nm). Gain

values were extracted by a fit of emission vs. stripe length to data the 1-D amplifier model, as originally proposed by Shaklee and Leheny. [32]

Fabrication of QD patterns: The patterning process used for fabricating QD patterns includes several stages. First, thinning solvent 700 was added to the OSCoR SL 1 resist solution to dilute it to half of the original concentration provided by the company. The diluted resist was spun cast on the silicon substrate to form a 400nm thick film (2000 rpm for 1 min). The cast film was baked at 100℃ for 1 min to remove the residual solvent. Short oxygen plasma etching (5 sec) was performed to improve the wettability of the OSCoR SL 1 film surface for the deposition of the negative photoresist (NR 71-3000 p). Ethyl lactate was added to the negative resist NR71-3000p solution to dilute it to one third of the original concentration provided by the company. The diluted resist was spun cast on top of OSCoR SL 1 film surface (3000 rpm for 1 minute). The cast film was subsequently soft baked at 100℃ for 5 minutes and exposed to 365 nm with a dosage of 123mW. The exposed film was then post-baked at 100℃ for 5 minutes and developed by soaking in RD6 developer for 5 sec.

After the development, the film was rinsed with water and dried by blowing with air.[23] Plasma etching (300W) with fixed gas flow at 45 sccm (O_2) and 5 sccm (Ar) was performed for 60 seconds in order to etch the underlying OSCoR SL 1 resist. $CsPbBr_3$ QD solution was spun cast (1000rpm for 1 minute) on the patterned templates. The sample was subsequently immersed into Orthogonal Stripper 700 for an hour to dissolve the OSCoR SL 1 resist and lift off the photoresist along with the attached $CsPbBr_3$ QD assemblies. To fabricate QD microdisk arrays, a low refractive index layer of CYTOP (n = 1.34, 1.5μm thick) was deposited on the Si wafer (n = 3.44) prior to the deposition of OSCoR SL 1 resist, in order to provide light confinement within the QD cavities.

Confocal PL configuration: The 450-nm output of the OPO was used to pump the samples. A pair of polarizers was used to control the pump fluence, while an iris was used to control the beam spot size. The pump is directed through a 40x (NA = 0.65) microscope objective using a dichroic mirror and focused on the sample. The emission is collected through the same objective, transmitted through the dichroic mirror and focused onto a 0.5-mm diameter

optical fiber coupled to a 1/2m spectrometer and CCD array (resolution = 0.29 nm) or collimated and projected onto a camera lens for fluorescence imaging. An additional long pass filter is used to further attenuate the reflected pump beam.

Atomic force microscopy: AFM images were collected using a Dimension Icon AFM microscope (Bruker) in tapping mode according to the usual procedure.[52] MikroMasch tips were used that had a spring constant of approximately 7 N/m. Scan sizes of 60 µm by 60 µm with a scan rate within 0.3-0.8 Hz.

Transmission electron microscopy (TEM): A transmission electron microscope, JEOL 100 CX-II operated at an accelerating voltage of 100 keV. TEM samples were prepared by diluting the purified QD solution 100 times with toluene. 5-10 µL of the diluted solution was then drop-cast on the TEM grid and allowed to dry completely.

Acknowledgements

Financial support is acknowledged from the Air Force Office of Scientific Research FA9550-14-1-0037 (Synthetic Photonics Multidisciplinary University Research Initiative), FA9550-16-1-0187, FA9550-17-1-0297, and GTRI IRAD I554L0030 (synthesis, fabrication and characterization of QD and photonic arrays); the U.S. Department of Energy, Office of Basic Energy Sciences, Division of Materials Sciences and Engineering Award # DE-FG02-09ER46604 (QD spectral characterization). M. J. Smith acknowledges the Science, Mathematics and Research for Transformation (SMART) scholarship funded by OSD-T&E, Defense–Wide/PE0601120D8Z National Defense Education Program (NDEP)/BA-1, N00244-09-1-0081.

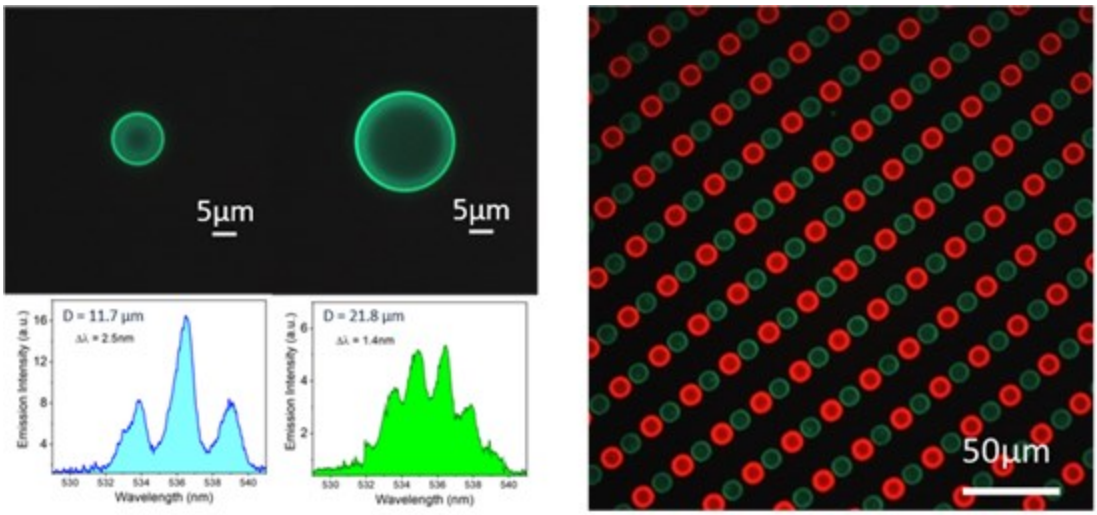

A novel orthogonal lithography process enables the fabrication of large-area and high-resolution arrays of various complicated all-inorganic perovskite QD patterns with smallest feature size down to several micron. Furthermore, QD microdisk lasers with tunable mode number and multicolor QD pixels on the same chip are demonstrated by utilizing this approach.

References

[1] N. S. Makarov, S. Guo, O. Isaienko, W. Liu, I. Robel, V. I. Klimov, *Nano Lett.* **2016**, 16, 2349.

[2] Y.-S. Park, S. Guo, N. S. Makarov, V. I. Klimov, *ACS Nano* **2015**, 9, 10386.

[3] J. Pan, S. P. Sarmah, B. Murali, I. Dursun, W. Peng, M. R. Parida, J. Liu, L. Sinatra, N. Alyami, C. Zhao, E. Alarousu, T. K. Ng, B. S. Ooi, O. M. Bakr, O. F. Mohammed, *J. Phys. Chem. Lett.* **2015**, 6, 5027.

[4] J. Pan, L. N. Quan, Y. Zhao, W. Peng, B. Murali, S. P. Sarmah, M. Yuan, L. Sinatra, N. M. Alyami, J. Liu, E. Yassitepe, Z. Yang, O. Voznyy, R. Comin, M. N. Hedhili, O. F. Mohammed, Z. H. Lu, D. H. Kim, E. H. Sargent, O. M. Bakr, *Adv. Mater.* **2016**, 28, 8718.

[5] X. Li, Y. Wu, S. Zhang, B. Cai, Y. Gu, J. Song, H. Zeng, Adv. Funct. Mater. 2016, 26, 2435.

[6] P. Liu, W. Chen, W. Wang, B. Xu, D. Wu, J. Hao, W. Cao, F. Fang, Y. Li, Y. Zeng, R. Pan, S. Chen, W. Cao, X. W. Sun, K. Wang, Chem. Mater. 2017, 29, 5168.

[7] L. Protesescu, S. Yakunin, M. I. Bodnarchuk, F. Krieg, R. Caputo, C. H. Hendon, R. X. Yang, A. Walsh, M. V. Kovalenko, *Nano Lett.* **2015**, 15, 3692.
[8] J. Jung, C. H. Lin, Y. J. Yoon, S. T. Malak, Y. Zhai, E. L. Thomas, V. Vardeny, V. V. Tsukruk, Z. Lin, *Angew. Chem.* **2016**, 128, 5155.
[9] G. Nedelcu, L. Protesescu, S. Yakunin, M. I. Bodnarchuk, M. J. Grotevent, M. V. Kovalenko, *Nano Lett.* **2015**, 15, 5635.
[10] S. Yakunin, L. Protesescu, F. Krieg, M. I. Bodnarchuk, G. Nedelcu, M. Humer, G. De Luca, M. Fiebig, W. Heiss, M. V. Kovalenko, *Nat. Commun.* **2015**, 6, 8056.
[11] T. L. Doane, K. L. Ryan, L. Pathade, K. J. Cruz, H. Zang, M. Cotlet, M. M. Maye, *ACS Nano* **2016**, 10, 5864.
[12] E. Yassitepe, Z. Yang, O. Voznyy, Y. Kim, G. Walters, J. A. Castañeda, P. Kanjanaboos, M. Yuan, X. Gong, F. Fan, J. Pan, S. Hoogland, R. Comin, O. M. Bakr, L. A. Padilha, A. F. Nogueira, E. H. Sargent, *Adv. Funct. Mater.* **2016**, 26, 8757.
[13] C.-Y. Huang, C. Zou, C. Mao, K. L. Corp, Y.-C. Yao, Y.-J. Lee, C. W. Schlenker, A. K. Y. Jen, L. Y. Lin, *ACS Photonics* **2017**, 4, 2281.
[14] N. Zhang, W. Sun, S. P. Rodrigues, K. Wang, Z. Gu, S. Wang, W. Cai, S. Xiao, Q. Song, *Adv. Mater.* **2017**, 29, 1606205.
[15] X. He, P. Liu, H. Zhang, Q. Liao, J. Yao, H. Fu, *Adv. Mater.* **2017**, 29, 1604510.
[16] J. Feng, X. Yan, Y. Zhang, X. Wang, Y. Wu, B. Su, H. Fu, L. Jiang, *Adv. Mater.* **2016**, 28, 3732.
[17] P. Liu, X. He, J. Ren, Q. Liao, J. Yao, H. Fu, *ACS Nano* **2017**, 11, 5766.
[18] Z. Gu, K. Wang, H. Li, M. Gao, L. Li, M. Kuang, Y. S. Zhao, M. Li, Y. Song, *Small* **2017**, 13, 1603217.
[19] S. Schünemann, K. Chen, S. Brittman, E. Garnett, H. Tüysüz, *ACS Appl. Mater. Interfaces* **2016**, 8, 25489.
[20] F. Palazon, Q. A. Akkerman, M. Prato, L. Manna, *ACS Nano* **2016**, 10, 1224.
[21] J. Chen, Y. Wu, X. Li, F. Cao, Y. Gu, K. Liu, X. Liu, Y. Dong, J. Ji, H. Zeng, *Advanced Materials Technologies* **2017**, 2, 1700132.
[22] T. S. Mentzel, D. D. Wanger, N. Ray, B. J. Walker, D. Strasfeld, M. G. Bawendi, M. A. Kastner, *Nano Lett.* **2012**, 12, 4404.
[23] C. H. Lin, Q. Zeng, E. Lafalce, M. J. Smith, S. T. Malak, J. Jung, Y. J. Yoon, Z. Lin, Z. V. Vardeny, V. V. Tsukruk, *Adv. Opt. Mater.* **2017**, 5, 1700011.
[24] Y. Kim, E. Yassitepe, O. Voznyy, R. Comin, G. Walters, X. Gong, P. Kanjanaboos, A. F. Nogueira, E. H. Sargent, *ACS Appl. Mater. Interfaces* **2015**, 7, 25007.
[25] S. Schünemann, K. Chen, S. Brittman, E. Garnett, H. Tüysüz, *ACS Appl. Mater. Interfaces* **2016**, 8, 25489.
[26] J. A. Castañeda, G. Nagamine, E. Yassitepe, L. G. Bonato, O. Voznyy, S. Hoogland, A. F. Nogueira, E. H. Sargent, C. H. B. Cruz, L. A. Padilha, *ACS Nano* **2016**, 10, 8603.
[27] J. De Roo, M. Ibáñez, P. Geiregat, G. Nedelcu, W. Walravens, J. Maes, J. C. Martins, I. Van Driessche, M. V. Kovalenko, Z. Hens, *ACS Nano* **2016**, 10, 2071.
[28] B. H. Kim, S. Nam, N. Oh, S.-Y. Cho, K. J. Yu, C. H. Lee, J. Zhang, K. Deshpande, P. Trefonas, J.-H. Kim, J. Lee, J. H. Shin, Y. Yu, J. B. Lim, S. M. Won, Y. K. Cho, N. H. Kim, K. J. Seo, H. Lee, T.-i. Kim, M. Shim, J. A. Rogers, *ACS Nano* **2016**, 10, 4920.

[29] S. Krotkus, F. Ventsch, D. Kasemann, A. A. Zakhidov, S. Hofmann, K. Leo, M. C. Gather, *Adv. Opt. Mater.* **2014**, 2, 1043.

[30] C. H. Lin, E. Lafalce, J. Jung, M. J. Smith, S. T. Malak, S. Aryal, Y. J. Yoon, Y. Zhai, Z. Lin, Z. V. Vardeny, V. V. Tsukruk, *ACS Photonics* **2016**, 3, 647.

[31] Y. Wang, X. Li, J. Song, L. Xiao, H. Zeng, H. Sun, *Adv. Mater.* **2015**, 27, 7101.

[32] K. L. Shaklee, R. F. Leheny, *Appl. Phys. Lett*. **1971**, 18, 475.

[33] A. Loiudice, S. Saris, E. Oveisi, D. T. L. Alexander, R. Buonsanti, *Angew. Chem. Int. Ed.* **2017**, 56, 10696.

[34] P. J. Yunker, T. Still, M. A. Lohr, A. G. Yodh, *Nature* **2011**, 476, 308.

[35] Y. Wang, K. E. Fong, S. Yang, Van D. Ta, Y. Gao, Z. Wang, V. Nalla, H. V. Demir, H. Sun, *Laser Photon. Rev.* **2015**, 9, 507.

[36] S. Yang, Y. Wang, H. Sun, *Adv. Opt. Mater.* **2015**, 3, 1136.

[37] R. C. Polson, G. Levina, Z. V. Vardeny, *Appl. Phys. Lett.* **2000**, 76, 3858.

[38] R. C. Polson, Z. V. Vardeny, D. A. Chinn, *Appl. Phys. Lett.* **2002**, 81, 1561.

[39] K. Park, J. W. Lee, J. D. Kim, N. S. Han, D. M. Jang, S. Jeong, J. Park, J. K. Song, *J. Phys. Chem. Lett.* **2016**, 7, 3703.

[40] T. J. S. Evans, A. Schlaus, Y. Fu, X. Zhong, T. L. Atallah, M. S. Spencer, L. E. Brus, S. Jin, X. Y. Zhu, *Adv. Opt. Mater.* **2018**, 6, 1700982.

[41] Z. Duan, Y. Wang, G. Li, S. Wang, N. Yi, S. Liu, S. Xiao, Q. Song, *Laser Photon. Rev.* **2018**, 12, 1700234.

[42] H. Hodaei, M.-A. Miri, M. Heinrich, D. N. Christodoulides, M. Khajavikhan, *Science* **2014**, 346, 975.

[43] J. Xing, X. F. Liu, Q. Zhang, S. T. Ha, Y. W. Yuan, C. Shen, T. C. Sum, Q. Xiong, *Nano Lett.* **2015**, 15, 4571.

[44] X. He, P. Liu, H. Zhang, Q. Liao, J. Yao, H. Fu, *Adv. Mater.* **2017**, 29, 1604510.

[45] S. W. Eaton, M. Lai, N. A. Gibson, A. B. Wong, L. Dou, J. Ma, L.-W. Wang, S. R. Leone, P. Yang, *Proc. Natl. Acad. Sci. USA* **2016**, 113, 1993.

[46] Y. Takubo, Y. Hisatake, T. Lizuka, T. Kawamura, *SID Symposium Digest of Technical Papers* **2012**, 43, 869.

[47] M. Kuang, J. Wang, B. Bao, F. Li, L. Wang, L. Jiang, Y. Song, *Adv. Opt. Mater.* **2014**, 2, 34.

[48] X. Tang, X. Tang, K. W. C. Lai, *ACS Photonics* **2016**, 3, 2396.

[49] W. K. Bae, M. K. Nam, K. Char, S. Lee, *Chem. Mater.* **2008**, 20, 5307.

[50] S. T. Malak, M. J. Smith, Y. J. Yoon, C. H. Lin, J. Jung, Z. Lin, V. V. Tsukruk, *Adv. Opt. Mater.* **2017**, *5*, 1600509.

[51] S. T. Malak, J. Jung, Y. J. Yoon, M. J. Smith, C. H. Lin, Z. Lin, V. V. Tsukruk, *Adv. Opt. Mater.* **2016**, 4, 608.

[52] M. E. McConney, S. Singamaneni, V. V. Tsukruk, *Polymer Rev.* **2010**, 50, 235.